Applied Catalysis B: Environmental 336 (2023) 122949

Contents lists available at ScienceDirect

Applied Catalysis B: Environmental

journal homepage: www.elsevier.com/locate/apcatb

Size-dependent and sensitivity of copper particle in ternary CuZnAl catalyst for syngas to ethanol

Yongjun Liu [a,*], Zhiwen Li [a], Peng Luo [a], Nan Cui [a], Kejing Wang [a], Wei Huang [a,b,**]

[a] State Key Laboratory of Clean and Efficient Coal Utilization, Taiyuan University of Technology, No.79, Yingze West Street, Taiyuan 030024, Shanxi, China
[b] Shanxi-Zheda Institute of Advanced Materials and Chemical Engineering, Taiyuan 030024, Shanxi, China

ARTICLE INFO

Keywords:
Cu-based catalyst
Syngas
Ethanol
Size effects
In-situ DRIFT

ABSTRACT

Understanding particle size effect of metal on catalysis has great significance in scientific and industrial applications. Herein, CuZnAl catalysts with narrow Cu particle size distribution had been synthesized and investigated for syngas to ethanol. Selectivity toward to $C_{2+}OH$ sharply increased from 8.9% to 60.5% with the increase of Cu size from 11.8 to 38.3 nm, then it slightly increased to 68.6% when further increasing the size to 49.2 nm, which was attributed to the domination of Cu (111) facet and accompanied by the formation of $Cu_{(111)}$-ZnO interface at larger Cu sizes, thereby weakened hydrogenation activity and facilitated CH_x formation. The *in-situ* DRIFTS experiment revealed that carbon chain growth was processed by the insertion of CO*/CHO* into the CH_x* and the coupling of CH_x* and CO_2 *. These results substantially broaden the understanding the size effect of Cu and provided guidance for design more active Cu-based catalyst for ethanol synthesis.

1. Introduction

Syngas (CO/H_2), which can be derived from gasification of biomass/coal or reforming of natural gas, is one of the most important platforms for supplying variable chemical feedstock and clean liquid fuels (or fuel additives) via Fischer-Tropsch synthesis. It is considered to be a promising strategy to deal with rising energy crisis as well as meet the increasing requirements of environmental protection [1–3]. In the past few years, this topic research area has been achieved great progress in the synthesis of light olefins [4], aromatics [5], gasoline/diesel [6] and so on. Compared with hydrocarbons, the synthesis of C_{2+} oxygenates, such as ethanol and higher alcohols (HA, $C_{2+}OH$), has more advantages because of the partial retention of C-O bond and higher atomic utilization [7,8]. The produced ethanol and $C_{2+}OH$ can be used as fuel additives to reduce emissions of NO_x, CO_2, feedstock for the synthesis of olefins, or as vital intermediate for manufacturing pharmaceuticals, cosmetics and detergents. Another important potential application for ethanol is that it can be used as hydrogen carriers and converted into hydrogen-rich gas for fuel cells. This cycle utilizes the efficiency of fuel cell power and eliminates the emission characteristics of traditional combustion process [9].

Typically, the higher alcohols synthesis (HAs) reaction requires dual active sites, in which one site functions for CO or CH_xO (x = 1–3) dissociation and alkyl species (CH_x) formation, while the other site act as CO/CH_xO non-dissociative adsorption and insertion into CH_x to form CH_xCO/CH_xCHO intermediate, ethanol and $C_{2+}OH$ are then formed after a subsequent hydrogenation process [10]. Due to the simultaneously requirement of C-C coupling and the retention some of C-O bonds, it is challenging to regulate the synergy between the dual active sites to obtain high selectivity of $C_{2+}OH$. Additionally, the alkyl species are more likely hydrogenated to generate hydrocarbons rather than coupling with CO/CH_xO intermediates, resulting in relative low selectivity and space-time yield to ethanol and $C_{2+}OH$, especially for catalysts containing Co or Fe [11,12]. Till now, Rh is reported the only metal that can produce ethanol and $C_{2+}OH$ with high selectivity from syngas. However, its exorbitant cost and scarcity make it impossible to meet large-scale application in ethanol and $C_{2+}OH$ production [12].

Cu-based catalysts have received extensive attention because of the low feedstock price. These catalysts are usually promoted with promoters such as alkali (Li, Na, K and Cs.) and/or transition metals (Fe, Co, Ru, etc.) which can enhance the formation of CH_x or the C-C coupling [12]. The selectivity of ethanol and $C_{2+}OH$ will be significantly reduced

* Corresponding author.
** Corresponding author at: State Key Laboratory of Clean and Efficient Coal Utilization, Taiyuan University of Technology, No.79, Yingze West Street, Taiyuan 030024, Shanxi, China.
E-mail addresses: liuyongjun@tyut.edu.cn (Y. Liu), huangwei@tyut.edu.cn (W. Huang).

https://doi.org/10.1016/j.apcatb.2023.122949
Received 18 March 2023; Received in revised form 6 May 2023; Accepted 31 May 2023
Available online 2 June 2023

if promoter is lacking. However, ethanol was found as an unexpected product when slurry CuZnAlOOH ternary catalyst was prepared by a complete liquid-phase (CLP) technology [13]. The subsequent researches confirmed that the ratio of $Cu^0/(Cu^0+Cu^+)$, AlOOH, the oxygen vacancies of ZnO_x and surface amount of acid greatly affected the catalytic performance [14–16]. However, the syngas conversion to ethanol and higher alcohols system was an extremely complex reaction process, which involved syngas to methanol, methanol dehydration to dimethyl ether (DME), F-T synthesis and water gas shift reaction (WGS), making it hard to understand the selectivity and mechanism. Several Cu facets and active sites were reported to be responsible for CO hydrogenation to ethanol and side-reactions [17–20]. For example, Wang's group reported that ethanol formation started with CO hydrogenation to CH_3O via CHO intermediate. The dissociation of CH_3O could produce CH_3, or directly hydrogenated to yield CH_3OH. CHO insertion into CH_3 to form CH_3CHO was the most favorable pathway in ethanol synthesis on Cu (211) facet [18], while Huang et al.[20] reported that $Cu_{(100)}$-hydroxylated ZnO ensemble and $Cu_{(611)}Zn$ alloy were the active sites for WGS and CO hydrogenation reactions, respectively. Recently, we had distinguished the structural differentiation between the Cu-based catalyst prepared by the CLP technology and the industrial methanol synthesis catalyst in detail. It was discovered that the hydrogenation step of CH_xO^* species to metahnol was inhibited on CuZnAlOOH catalyst when it was prepared by CLP technology, and the active Cu size of the former was much greater than that of the latter [21].

There's no doubt that the size and morphology of metal nanoparticles are important factors affecting the behavior of catalysts in heterogeneous catalysis, which determines the distribution of the active sites. Therefore, the effect of particle size of active components on the catalytic behavior for syngas conversion also has been widely studied in recent years. So far, different conclusions about size effects have been reported. Natesakhawat et al.[22] reported that CO_2 hydrogenation to methanol was a structure-sensitive reaction and found that smaller Cu particles showed higher TOF values. A contradicting conclusion was achieved by Karelovic who proposed that catalysts with large Cu and ZnO particles forming new active sites, resulting in a very high methanol synthesis activity and selectivity [23]. In addition, ZnO crystal size of OX-ZEO bifunctional catalyst was also reported to influence both CO conversion and light olefins selectivity in the range of 23–79 nm because smaller particles possessed a higher specific surface area [24]. The effect of particle sizes was also studied in cobalt-supported catalysts for F-T reaction. Dai et al.[25] discovered that the Fischer-Tropsch to olefins performance was independent of Co_2C particle size when the size was larger than 7 nm, whereas both intrinsic activity and product distribution were depended on the Co_2C particle size when it was smaller than 7 nm. Similar results were also achieved for other cobalt-supported catalysts.

Because of the remarkable structural differentiation for methanol synthesis and ethanol/C_{2+}OH synthesis over different CuZnAl catalyst, the size effect of Cu nanoparticles under realistic CO hydrogenation reaction should be thoroughly investigated. Understanding of this aspect would lead to design of more efficient catalysts. Therefore, we focused on the particle size effect of Cu derived from $CuZnO_xAlOOH$ on catalytic performance for syngas to ethanol and C_{2+}OH in this study. The particle size of Cu was modulated by adjusting Cu/Zn ratios when the catalysts were prepared by CLP technology.

2. Experimental

2.1. Catalyst preparation

The CuZnAl catalysts with varying Cu particle sizes were synthesized by the CLP method as in our previous work [21], where Cu nanoparticles with different sizes were achieved by changing Cu or Zn content. In brief, a certain amount of aluminum isopropoxide $(C_3H_7O)_3Al$ was added into 100 mL of 0.033 M aqueous solution of citric acid and pre-hydrolyzed at 323 K for 3 h. Then the temperature was raised up to 368 K for further hydrolysis under vigorous stirring. After 0.5 h, a mixed nitrate solution ($Cu(NO_3)_2{\cdot}3\,H_2O$, $Zn(NO_3)_2{\cdot}6\,H_2O$ and ethylene glycol) with varying Cu or Zn content was added dropwise into the above Al sol and stirred at 368 K until a highly viscous gel was formed. The gel was further dispersed into 300 mL of liquid paraffin (LP) and heated to 573 K for 8 h with a heating rate of 1 K/min under N_2 flow to obtain the slurry catalysts. Catalysts were labelled as Cu*x* or Zn*y* with *x* and *y* representing to the molar ratio of Cu and Zn, respectively.

2.2. Catalyst characterization

The slurry catalysts were centrifuged and extracted by petroleum ether, then dried at room temperature to achieve the solid power before characterization.

XRD patterns were recorded on a Rigaku Smartlab equipped with Cu Kαradiation (40 kV, 40 mA) in the 2θ range of 5°~85°. The Cu^0 crystal sizes were calculated by the Scherrer equation and were averaged for comparison according to strongest diffraction peaks at 43.3°, 50.4° and 74.1°, respectively.

The composition of Cu, Zn and Al was measured by Agilent ICP-OES 730 inductively coupled plasma emission spectrometer (ICP).

H_2-TPR experiment was performed on TP-5080 chemisorption instrument. 50 mg of sample was firstly swept at 423 K for 30 min in a flow of He atmosphere. After cooling down to 323 K, the gas was switched to 5% H_2-95% Ar (30 mL·min^{-1}) and the temperature was raised from 323 to 773 K with a rate of 10 K·min^{-1}. The H_2 consumption was detected from 323 K to 773 K using a thermal conductivity detector (TCD).

N_2 adsorption-desorption patterns were recorded on a Quantachrome QDS-30 instrument. Before each measurement, all samples were degassed in vacuum at 473 K for 4 h, the isotherms were then recorded at 77 K. The Brunauer-Emmett-Teller (BET) method was applied to calculate the specific surface area and pores volume.

The copper dispersion (D_{Cu}) and copper surface area (S_{Cu}) were measured by N_2O titration [26]. Generally, 100 mg of samples were firstly reduced in flowing 5%H_2-95%N_2 of 30 mL·min^{-1} at 523 K for 30 min. After cooling down to room temperature, a mixture of 5%N_2O-N_2 (30 mL/min) was switched to oxidize surface Cu^0 to Cu^+, and the sample was then flushed with N_2 for 30 min to remove the excess N_2O. Finally, the Cu^+ on catalyst surface was reduced again and the H_2 consumption (*X*) was confirmed. The D_{Cu} and S_{Cu} values were calculated by the following equation:

$$D_{Cu} = 2X \times \frac{M_{Cu}}{W_{Cu}} \times 100\% \quad (1)$$

$$S_{Cu} = 2 \times X \times N_{av} / (1.4 \times 10^{19}) \quad (2)$$

Where M_{Cu} was the Cu relative atomic mass, W_{Cu} was the actual Cu loading calculated by ICP, N_{av} was the Avogadro constant, and 1.4×10^{19} was the number of copper atoms per m^2.

XPS was carried out using ESCALAB 250 energy spectrometer equipped with an Al Kα X-ray radiation source ($h\nu$ =1486.6 eV) under a high vacuum. The C1*s* spectral peak (284.8 eV) was taken as the reference to calibrate the binding energy.

Raman patterns were recorded using a Raman spectrometer (HORIBA LabRAM HR) equipped with a ventus laser. The spectrometer was equipped with a 50 × telephoto lens and a visible 325 nm UV laser as the light source. The exposure time and the scanning frequency were 10 s and 2 times, respectively.

TEM images were collected on a JEM-2100 F instrument with a 200 kV acceleration voltage. Before test, samples were ultrasonically dispersed in ethanol solutions, then it was deposited on carbon-coated copper grid for measurement.

2.3. Catalytic activity measurements

The catalytic activity measurements were performed on a 0.5 L continuous stirred slurry autoclave reactor. About 20 g of catalysts dispersing in 300 mL of liquid paraffin were loaded into the slurry reactor. H_2 and CO were controlled by mass flow controllers and were introduced into the reactor with the GHSV of 450 mL·g_{cat}·h^{-1} until the pressure was elevated to 4.0 MPa and temperature reached up to the desired values. The effluent gas, after passing through a cold trap, was analyzed online by a Haixin GC-950 equipped with a FID and TCD detector. H_2, CO, CH_4, CO_2 were analyzed by the TCD detector connected to a TDX-01 column. The lower hydrocarbons were analyzed by a FID detector connected to a Porapak Q column. The liquid alcohols collected from cold trap were analyzed off-line per 24 h. All catalysts activity data were obtained after more than 24 h of stabilization. The CO conversion (X_{CO}) and product selectivity (Sel_i) were calculated according to the following two equations:

$$XCO = \frac{F_{inlet} - F_{outlet}}{F_{inlet}} \times 100\%$$

$$Sel_i = \frac{C_i \times n_i}{\sum C_i \times n_i} \times 100\%$$

where F represented the molar flow of CO in the gases, C_i indicated the molar fraction of product *i*, (CH, CO_2 and ROH), and n_i was the carbon number of product *i*.

3. Results and discussion

3.1. Catalyst characterization

The textural property of different fresh and spent catalysts was characterized by N_2 adsorption. All catalysts exhibited a type IV isotherm with H3 hysteresis loop (Fig. S1), suggesting mesopores structure existed in all slurry CuZnAl catalysts. Overall, the BET surface area (S_{BET}) of fresh catalysts increased when increasing Cu or decreasing Zn proportions (Table 1). After measured by the ICP to determine the actual loading of Cu, it was interesting to discover that the BET surface area of the fresh catalyst increased at a nearly linear rate from 30.5 to 90.8 $m^2 \cdot g^{-1}$ as a function of Cu loading (Fig. S2). After reaction, the two values of S_{BET} and V_P significantly increased, while the D_p value reduced, which was a common feature for catalysts prepared by the CLP technology [27]. This was mainly due to the fact that the special preparation method caused a very small amount of liquid paraffin (LP) adsorbed in the small pores during the heat treatment of gel in liquid paraffin, then this adsorbed LP would be removed gradually during reaction [27,28].

The XRD patterns of the various fresh CuZnAl catalysts were shown in Fig. S3, and the diffraction peaks appearing at 43.4, 50.5, and 74.1° were assigned to diffractions of the (111), (200), and (220) facet of metallic Cu^0. No evident diffraction characteristic peaks of Cu^+ or Cu^{2+} were found, which was further proved by the XPS spectra [29]. In addition, a poor peak of free carbon appeared at 28.7°, which was due to the CLP method causing partial decomposition of LP during liquid phase heat treatment, and thus resulting in the reduction of Cu species [30]. Also, no characteristic peaks associated with Al and Zn species could be identified, suggested that they were highly dispersed on catalysts. The average Cu crystallite sizes of various CuZnAl catalysts were determined using Scherrer formula and displayed in Table 1, one could see that the size varied from 32.3 to 36.4 nm depending on the Cu content. These values were much larger than that of commercial syngas-to-methanol synthesis catalysts (~10 nm) [31], and provided us opportunities to explore the size-dependent catalytic behavior of CuZnAl catalyst for ethanol investigation.

TEM was further applied to determine the Cu particle size of catalysts. As shown in Fig. 1, the average Cu particle size (dark area) of the catalysts was found to be widely distributed in the range of 32.4–49.2 nm. Overall, the Cu particle size was also observed increasing with Cu loading. And the sizes obtained from the XRD and TEM characterizations showed the same variation trend (see Fig. 1K), that was, the particle size was related to the crystallite size, i.e., the larger the particles, the larger the crystallites. Besides, one could see that the Cu particle size measured from the TEM images were greater than that of calculated by the XRD, which was probably.

due to the fact that the exposed facet of Cu particle size in TEM was dominated by Cu (111) (see Fig. 1A), while crystallite sizes were obtained by the average of (111), (200), and (220) facets. The lattice fringes with D-spacing of approximately 2.08 and 2.47 Å corresponded to the Cu^0 (111) and ZnO (002) facet, respectively, further confirmed the above conclusion. Notably, the interface between Cu (111) and ZnO (002) could be clearly resolved in the nanoparticles (Fig. 1B). It should be noted that the C element also could be detected around the Cu particle, which was well consistent with the XRD and following Raman results. TEM observation suggested that there were larger Cu particle sizes exposure (111) facet in the catalyst and was accompanied by the formation of $Cu_{(111)}$-ZnO interface. In order to shed light on the relationship between Cu particle size and the catalytic performance, subsequent discussions were mainly based on the size of TEM results.

Raman spectrum was further indicated the absence of CuO phase on the catalyst (Fig. S4) since no Cu-O and Cu-O-Cu bonds located at about 295, 342 and 627 cm^{-1} were detected [32]. The peak at about 576 cm^{-1} and 1148 cm^{-1} were attributed to the $LO(A_1)$ and $LO(A_2)$ phonon mode from ZnO phase, respectively [33,34]. In addition, two evident peaks at around 1368 and 1606 cm^{-1} were corresponded to the defect-derived D-band and ordered graphite structure-derived G-band, respectively. The D-band was related to defects caused by disordered phase and lattice mismatch of the graphite layer, while the G-band was the $E_{2\,g}$ mode that

Table 1
Main physiochemical properties of different CuZnAl catalysts.

Catalyst	Cu^0 crystal size (nm)[a]	Particle sizes (nm)[b]	Before reaction[c]			After reaction[c]		Loading (*wt.*%)[d]			Cu/Zn[d]
			S_{BET} (m^2/g)	V_P (cm^3/g)	D_P (nm)	S_{BET} (m^2/g)	V_P (cm^3/g)	D_P (nm)	Cu	Zn	Al	
Cu2.0	32.3	32.4	30.5	0.14	16.4	114.2	0.28	11.6	30.6	15.8	3.8	2.0
Cu2.5	32.9	36.3	34.6	0.12	17.1	94.9	0.24	12.0	35.9	14.6	3.2	2.5
Cu3.0	33.5	42.3	35.9	0.14	21.2	84.4	0.22	13.8	38.0	13.2	4.5	2.9
Cu3.5	36.1	45.3	53.2	0.19	20.7	75.0	0.25	18.2	38.2	11.8	3.3	3.3
Cu4.0	36.3	47.2	56.8	0.19	19.3	85.4	0.22	15.3	40.3	11.7	2.8	3.5
Zn0.25	34.1	38.3	90.8	0.27	16.3	157.0	0.42	14.4	63.2	4.9	6.8	13.2
Zn0.5	36.4	49.2	59.9	0.19	19.0	110.2	0.32	16.4	51.0	7.1	5.0	7.3
Zn1.25	35.1	47.5	53.5	0.23	23.9	72.6	0.21	13.7	46.0	16.6	2.6	2.8
Zn1.5	36.3	44.3	43.2	0.18	20.4	65.0	0.23	18.0	40.5	15.9	4.0	2.6

[a] The average crystallite sizes were estimated by the Scherrer equation.
[b] The particle sizes were measured by TEM.
[c] S_{BET}, V_p, and D_p were determined by N_2 adsorption.
[d] Cu, Zn and Al loadings were measured by ICP-OES.

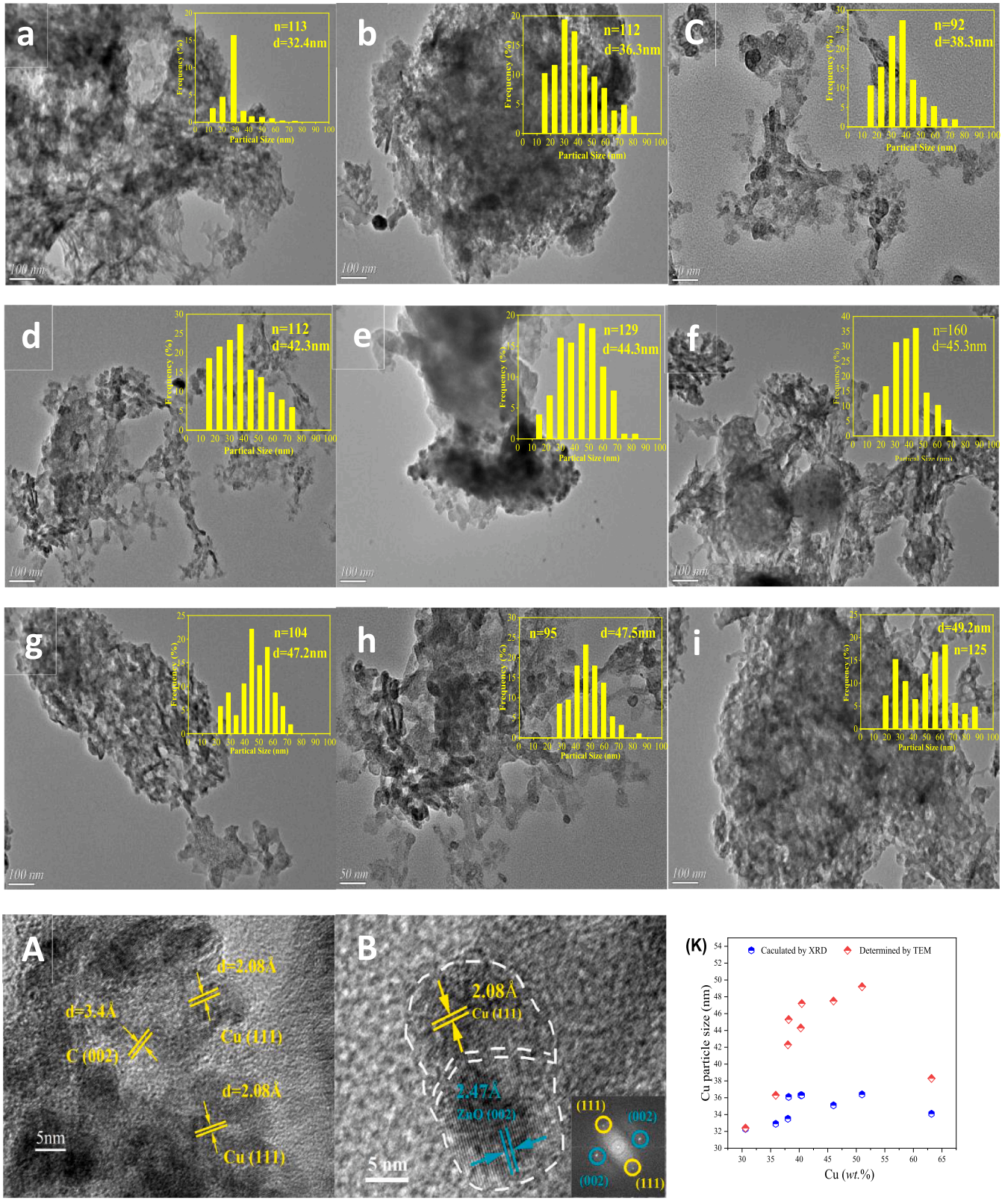

Fig. 1. TEM images and size distributions (insert) of CuZnAl catalysts with different Cu particle size; (a) Cu2.0; (b) Cu2.5; (c) Zn0.25; (d) Cu3.0; (e) Zn1.5; (f) Cu3.5; (g) Cu4.0; (h) Zn1.25 and (i) Zn0.5.

had stretching vibrations of sp^2 C-C bonds [35]. These results were consistent with the above XRD results.

3.2. Catalytic performance

The CO hydrogenation on CuZnAl catalysts with various Cu particle sizes and the commercial methanol synthesis catalyst (11.8 nm) were tested under the conditions of 250 °C, 4.0 MPa, $H_2/CO = 2.0$, 150 mL·min^{-1} and the results were summarized in Table 2 and plotted in Fig. 2. As seen, the Cu particle size significantly affected the alcohols distribution. For example, the higher alcohols ($C_{2+}OH$) selectivity was found to rapidly increasing from 8.9% to 60.5% with the increase of Cu particle size from 11.8 to 38.3 nm, then it slightly increased to the value of about 68.6% when further increasing the Cu particle size to 49.2 nm. However, the methanol (MeOH) selectivity followed a reverse trend, it decreased from 91.1% to 31.5% when the Cu particle size increased from 11.8 to 49.2 nm (Fig. 2A). Thus, the ratio of $C_{2+}OH$ to methanol simultaneously increased from 0.29 to 2.19 with the increase of Cu particle size (Fig. 2B). Moreover, increasing Cu particle size not only raised the selectivity of ethanol (ETOH), but also increased the $C_{3+}OH$ selectivity, and the influence of ethanol selectivity was greater than that of $C_{3+}OH$ (Fig. 2C). These results suggested that the capability of chain growth was enhanced with the increase of Cu particle size, and had more pronounce in the formation of initial C-C bond.

The experimental results also demonstrated that the Cu particle size influenced the CO conversion, the selectivity of total alcohols (ROH) and hydrocarbon (CH_x) (Fig. 3A∼C). Figs. 3A and 3B showed that both the CO conversion and ROH selectivity seemed not show a very clear dependence on the particle size, but slightly decreased with the increase of Cu particle size overall. In comparison, the CH_x selectivity increased simultaneously at larger Cu particle size. These results demonstrated that larger Cu particle size favored the formation of CH_x, whereas smaller ones favored to improve the activity. In general, particle size would affect the proportion of low index (111) and (100) planes, interfacial area between active site and support, angle atoms and edge atoms, which would in turn affect the electronic properties and surface structure of catalysts [36,37]. It was reported that smaller Cu particles contained larger numbers of open planes, edge/defect sites which were typically more reactive for the formation of methanol from CO and CO_2 hydrogenation according to literatures [22,38,39], which were consistent with our results. Compared with commercial methanol synthesis catalyst (11.8 nm), the larger Cu particle size prepared by the CLP method illustrated that in larger sizes, the Cu structure had been significantly modified, creating new active sites for the formation of ethanol and $C_{2+}OH$. The catalytic stability of representative catalyst (∼47.5 nm) as a function of time on stream were tested and showed in Fig. 3D. At beginning, relative higher selectivity of $C_{2+}OH$ was observed when syngas was introduced, then it gradually decreased to about 50 *wt.*% within 120 h, while the CO conversion was relative constant during 500 h reaction. After comparing the characterization results of the fresh and spent catalyst, it was found that the copper particle size measured from TEM images decreased to 40.2 nm (Fig. S5), the XRD result also confirmed the conclusion (Fig. S6), indicating the fact that the reduction of Cu^0 particle size led to the decrease of $C_{2+}OH$ selectivity. In addition, one could see that the selectivity of CO_2 increased, while the ROH selectivity decreased after 370 h, the XPS results showed that part of ZnO_x had been formed in the fresh catalyst, and the ratios of ZnO_x significantly increased to 0.47 after reaction (Fig. S7A). Besides, the oxygen defects (531.6 eV) could be easily deconvoluted on the O1*s* spectra (Fig. S7B). It was reported that the interface active site was probably the active center for WGS reaction, and the oxygen vacancy (O_v) could accelerate the dissociation of water [40,41]. Thus, it was highly speculated that the reason for the increase in CO_2 selectivity was ascribed to the increase of O_v in ZnO_x. The above catalytic performance results further indicated that syngas to $C_{2+}OH$ process over Cu-based catalyst was an extremely size-dependent reaction.

The correlation between product selectivity dependent on Cu particle size was compared in Fig. 4A and 4B. It was found that the selectivity of CH_x and $C_{2+}OH$ showed the same trend with the increase of Cu particle size, but an opposite trend was discovered for dimethyl ether (DME). It was well known that the synthesis of $C_{2+}OH$ always accompanied by the formation of hydrocarbon and CO_2 through F-T process and water gas shift reaction, respectively. In which the adsorbed CO firstly occurred dissociation and chain propagation to form surface alkyl species (CH_x*) [12]. The competitive reactions are the termination by hydrogenation and dehydrogenation of surface alkyl species to give hydrocarbon (including paraffin and olefins), or via CO insertion to yield alcohols. Thus, it was highly supported that the formation of alcohols and hydrocarbons not only competed with each other, but also share the common intermediates in some steps of the mechanisms. Combined with the changed trend of DME, CH_x, and $C_{2+}OH$, it was suggested the formation of $C_{2+}OH$ required abundant of CH_x* species, that was to say, the formation of $C_{2+}OH$ and CH_x were two mainly parallel reactions, while the formation of DME and ethanol/$C_{2+}OH$ was mainly dominated by competition. In addition, one could see that the yield of higher alcohol increased at larger particles overall (Fig. 4C), further suggesting the formation of higher alcohol was dependent on the Cu particle size.

Since the exactly active sites under the reaction conditions were not known so far, thus, the influence of the Cu particle size on the apparent activation energy (E_a) was determined by calculating the rate of CO conversion under different temperature. The logarithm of the rate constants (*k*) was plotted with the reciprocal temperatures (1000/RT) and a relationship between ln*k* and 1000/RT was established for each catalyst (Fig. S8). It was found that the values of E_a determined from the above procedure also plotted against the Cu particle size (Fig. 4D). The E_a value sharply increased from 58 to above 90 kJ/mol with the increase of Cu particle size from 32.4 to 42.3 nm, then it became relative stable at larger Cu particle size overall.

3.3. Chemical properties and reaction mechanism

H_2-TPR was applied to study the reduction behavior of various fresh

Table 2
Catalytic activity and product selectivity of syngas to higher alcohols over CuZnAl under conditions of 250 °C, 4.0 MPa, $H_2/CO = 2.0$, 150 mL·min^{-1}.

Particle sizes (nm)	CO. Conv. (%)	Carbon balance	Selectivity (mol.%)				ROH distribution (*wt.*%)					β/α + β (%)	D_{Cu} (%)	S_{Cu} (m^2/g_{cat})
			ROH	HC	DME	CO_2	C1	C2	C3	C4	C5			
11.8	28.9	1.01	44.3	10.1	0.4	45.2	91.1	3.6	2.7	2.1	0.4	—	25.4[21]	71.4[21]
32.4	9.8	0.99	32.9	4.6	23.2	39.3	77.2	11.6	3.3	4.5	3.3	38.7	3.9	8.1
36.3	11.2	1.01	30.5	5.4	21.9	42.1	73.5	13.9	4.4	4.3	3.9	43.0	3.5	8.5
38.3	8.1	0.97	36.7	39.4	0.9	23.0	39.5	38.4	7.0	5.8	9.3	70.8	2.9	12.1
42.3	8.0	0.99	32.0	45.5	0.4	22.1	45.5	28.2	8.8	8.7	7.7	70.1	1.9	4.7
44.3	8.9	0.97	28.0	36.4	0.2	35.2	33.2	46.1	7.3	6.7	6.6	61.5	2.2	5.8
45.3	8.0	0.98	29.0	44.6	0.4	25.9	33.8	35.7	8.4	11.6	10.5	80.5	2.0	5.0
47.2	6.2	0.99	19.5	27.0	1.2	52.4	36.3	42.4	8.1	6.8	6.4	74.2	3.0	8.1
47.5	11.7	0.96	30.3	41.6	0.5	27.5	35.2	39.7	8.4	7.5	9.3	69.3	1.7	5.2
49.2	7.9	0.96	36.8	38.5	0.3	24.5	31.4	38.8	6.3	11.9	11.6	65.7	1.9	6.4

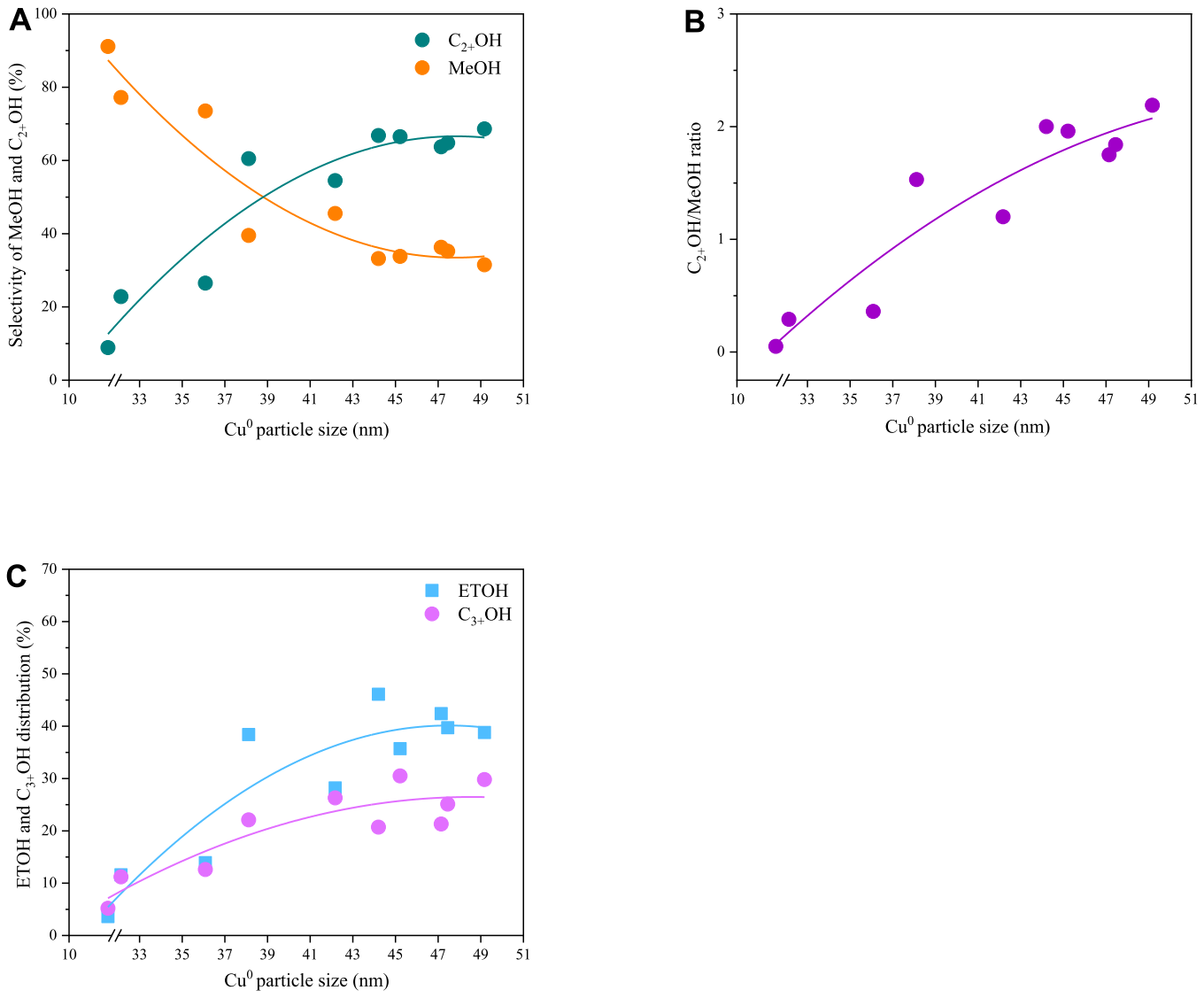

Fig. 2. Size-dependent of alcohols distribution corresponding to the data given in Table 2. (A) Distribution of $C_{2+}OH$ and methanol; (B) Ratio of $C_{2+}OH$ and methanol; (C) Distribution of ethanol and $C_{3+}OH$.

CuZnAl catalysts. As shown in Fig. 5, all catalysts showed two reduction peaks within the temperature range, indicating two kinds of reducible copper existed in catalysts. The lower temperature reduction peak (peak α) appearing at about 260 °C was ascribed to the reduction of surface Cu^+ to Cu^0 according to the following XPS characterization. In general, copper particles with smaller size were easier to be reduced than larger ones due to the interaction between the Cu species and carrier. Gao et al. [42] reported that the agglomeration of Cu species to form larger one would lead to the increase of the reduction temperature. Farahan et al. [43] also reported that the TPR peak temperature increased with the increase of CuO particle size, mainly due to the increasing ratio of bulk to surface CuO, with the latter required higher reduction temperature. Thus, it was highly speculated that the higher temperature peak (peak β) at around 400 °C was corresponded to the reduction of Cu^+ species in bulk with larger size. The consumption of H_2 for peak α and peak β were calculated and the results were displayed in Table S1, while the ratios of β/α + β were listed in Table 2 and Fig. 5 as a function of the Cu particle size. One could see that the contributions of peak β to the TPR pattern increased as the Cu particle size, then the values also became relative stable overall, which suggested that the catalyst with larger Cu particle size possess a greater proportion of harder reduced Cu^+ species.

According to the previous studies, the copper surface area (S_{Cu}) was reported to be an important factor for the catalytic performance of CO or CO_2 hydrogenation to methanol over Cu-based catalysts [22,44,45]. In our study, although the Cu particle size was not completely linear with the Cu dispersion (D_{Cu}) and specific surface area (S_{Cu}), it was still could be found that both the D_{Cu} and S_{Cu} slightly decreased with the increase of Cu particle size overall (Fig. S9), which was similar to that of CO conversion. This phenomenon was regarded that larger S_{Cu} favored the dissociative adsorption of H_2 on surface Cu sites, and consequently benefitted to the carbon-containing species hydrogenation reaction [45]. Herranz et al.[46] proposed that the limiting factor in H_2 adsorption was the availability of large ensembles of Co atoms on the surface of the nanoparticles for CO hydrogenation reaction. According to our previous study, it was also discovered that the CH_3O^* hydrogenation process was inhibited and thus the retention time of CH_3O^* was prolonged on catalyst surface using the CO + H_2 in-situ DRIFTS experiments [21]. Therefore, it could be concluded that the increase of Cu particle size was conducive to the generation of some new active sites, which limited the hydrogenating property of the catalysts and enhanced the C-C coupling capacity.

XPS analysis was carried out to distinguish the copper chemical valence states on the catalyst surface. As shown in Fig. S10, the binding energies (B.E.) of Cu2$p_{1/2}$ and Cu 2$p_{3/2}$ peak at ~952.0 and ~932.2 eV,

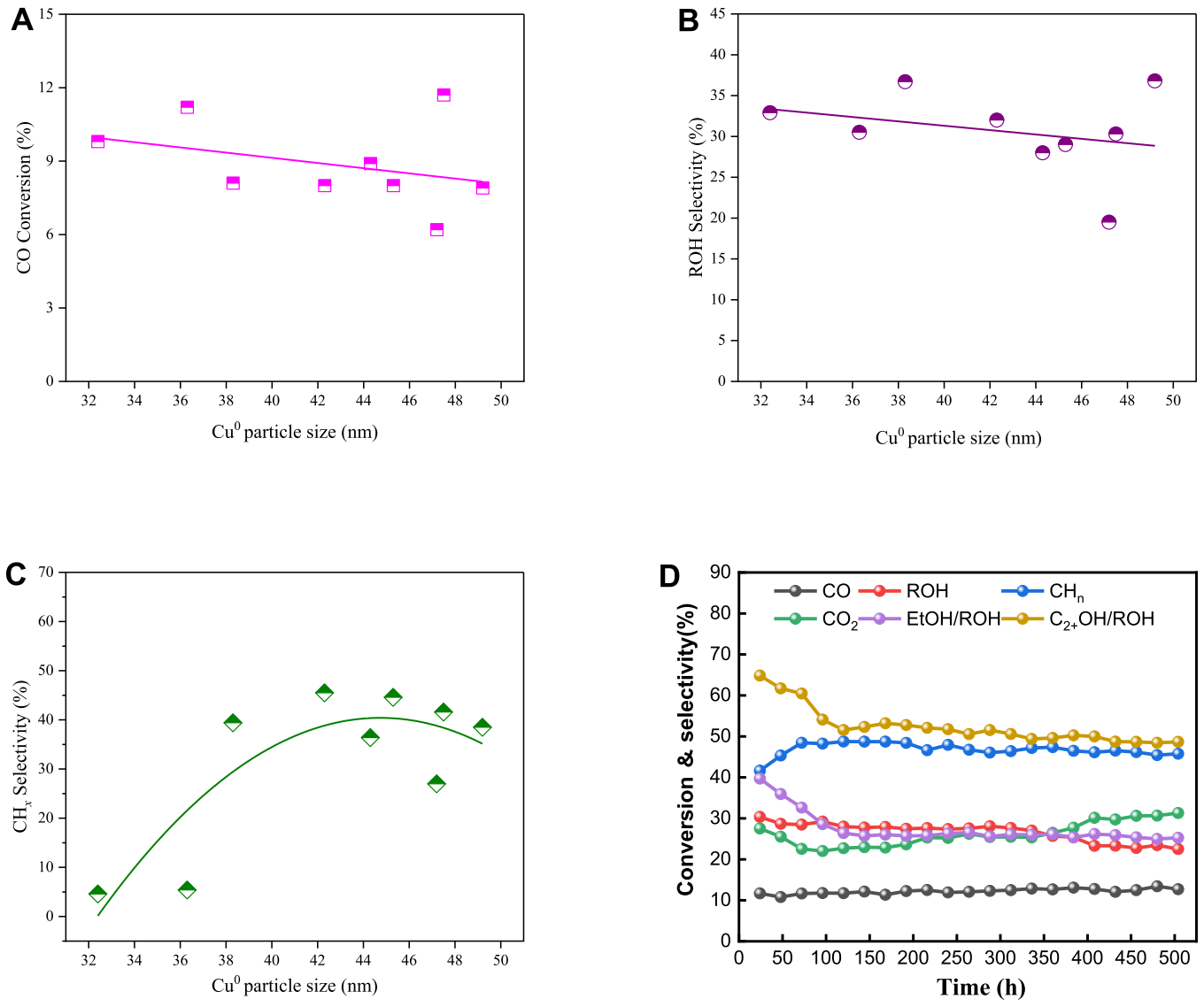

Fig. 3. Size-dependent activity of Cu particle on CO hydrogenation to ethanol. (A) CO conversion; (B,C) Product selectivity; (D) The stability of the representative catalyst (47.5 nm).

and no satellite peak between 940 and 948 eV were observed, indicating Cu^{2+} sites had been reduced into Cu^0 and/or Cu^+ over the fresh catalyst [22], which was in accordance with the previous XRD results. To identify the surface Cu^+ and Cu^0 species, Cu LMM X-ray excited Auger spectroscopy was analyzed. The appearance of two overlapping peaks at around 916.6 eV (Cu^+) and 918.6 eV (Cu^0) indicated the co-existence of Cu^0-Cu^+ species on catalyst surface (Fig. 6) [22]. After deconvolute the Cu LMM peaks to determine the surface Cu^0/Cu^+ species, one could see that the proportion of surface Cu^0 gradually increased with an increase in the particle size from 21% at 32.3 nm to about 55% at larger particle sizes. The XPS results confirmed the trend that the catalysts with larger Cu particle sizes had lower amount of surface Cu^+, which was also in accordance with the above TPR analyses.

To gain more insight into the CO adsorption behaviors of catalyst with different Cu particle size, three representative catalysts with Cu particle size of 32.4 nm, 42.3 nm and 47.5 nm were respectively studied by the *in-situ* CO-DRIFT spectra. As seen in Fig. 7, two distinct peaks located at 2176 cm^{-1} and 2116 cm^{-1} were observed for all catalysts, which were ascribed to the absorption of gaseous CO and linearly adsorbed CO on Cu sites [47]. After flushing with Ar flow at room temperature for 1 min, 3 min, 5 min, 7 min and 9 min, both the intensity of the two peaks reduced. It was reported that the vibrational bands of CO adsorption on the flat crystal plane varied with the CO coverage [48]. Therefore, the peak at 2176 cm^{-1} was attributed by CO adsorbed on the metallic Cu plane facet with a large number of contiguous Cu atoms. Furthermore, it was reported that the linear adsorption of CO on Cu^+ exhibited higher stability than that of Cu^{2+} and Cu^0 sites [49,50]. And the peak at 2116 cm^{-1} was independent of CO coverage, resulted from the CO adsorbed on step or corner sites of Cu particle. Thus, the peak centered at 2116 cm^{-1} in catalyst probably attributed to Cu^+-CO adsorbed on step or corner sites. Importantly, an additional peak at around 2000 cm^{-1} could be observed comparing with commercial CuZnAl methanol synthesis catalyst [21], and this peak remained stable after 9 min Ar sweeping. It was speculated that this characteristic peak was due to CO adsorption on the Cu-ZnO_{1-x} interface at the bridging position, or on metallic Cu sites where electronic modification occurred after interaction with ZnO_{1-x} [51]. According to the literature [52,53], this bridge-adsorbed CO was thought to be more easily cleaved, thereby forming the key intermediate of alkyl species (CH_n*) over Cu modified F-T synthesis catalysts or Rh-based catalyst. In addition, the intensity of this peak was enhanced with the increase of Cu particle size (Fig. 7D). This was consistent with the results of Arakawa

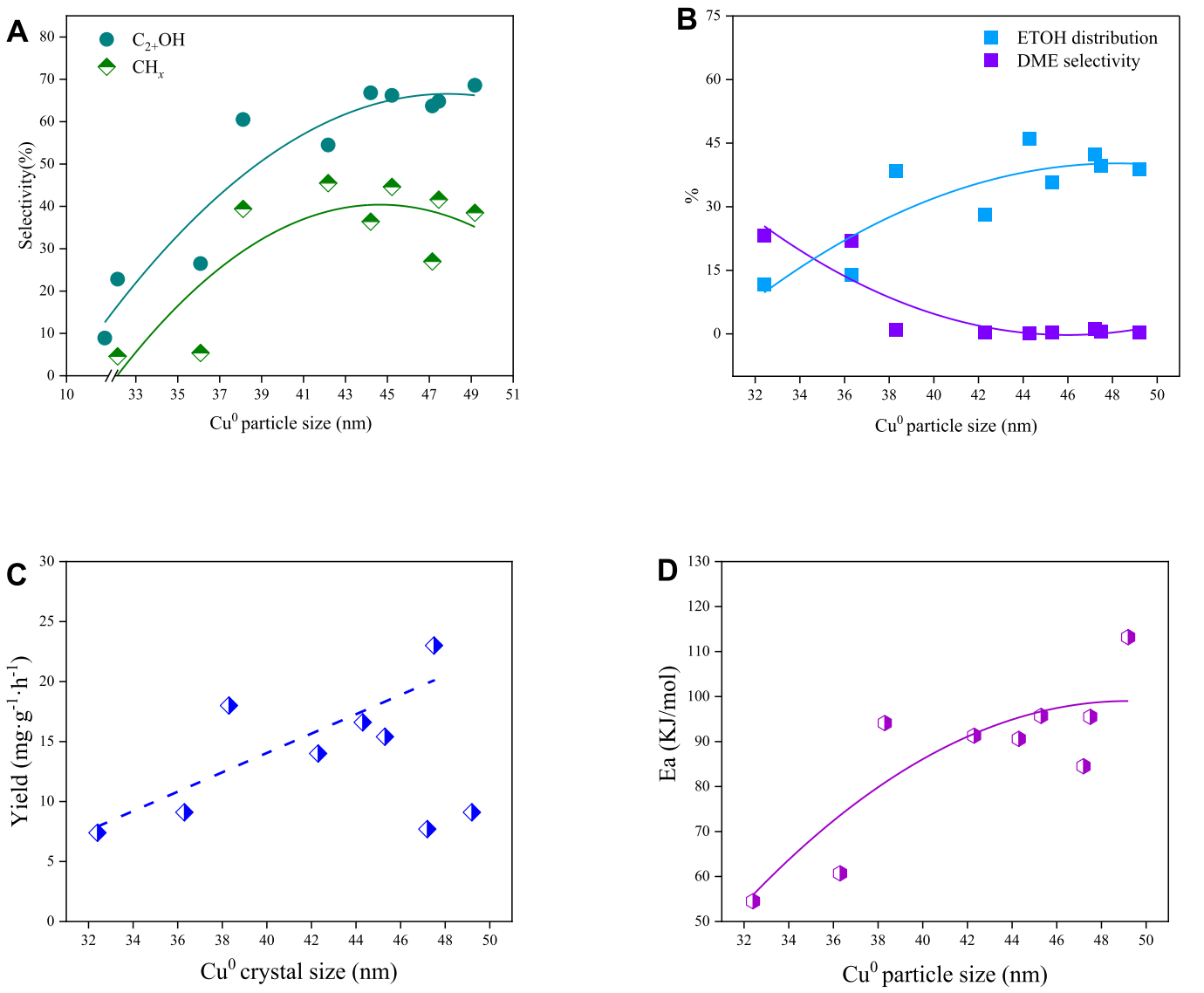

Fig. 4. Correlation between product selectivity dependent on Cu particle size corresponding to the data given in Table 2. (A) Selectivities of $C_{2+}OH$ and CH_x; (B) Selectivities of ETOH and DME; (C) Yield of higher alcohols; (D) Apparent activation energy over various CuZnAl catalysts as a function of Cu particle size.

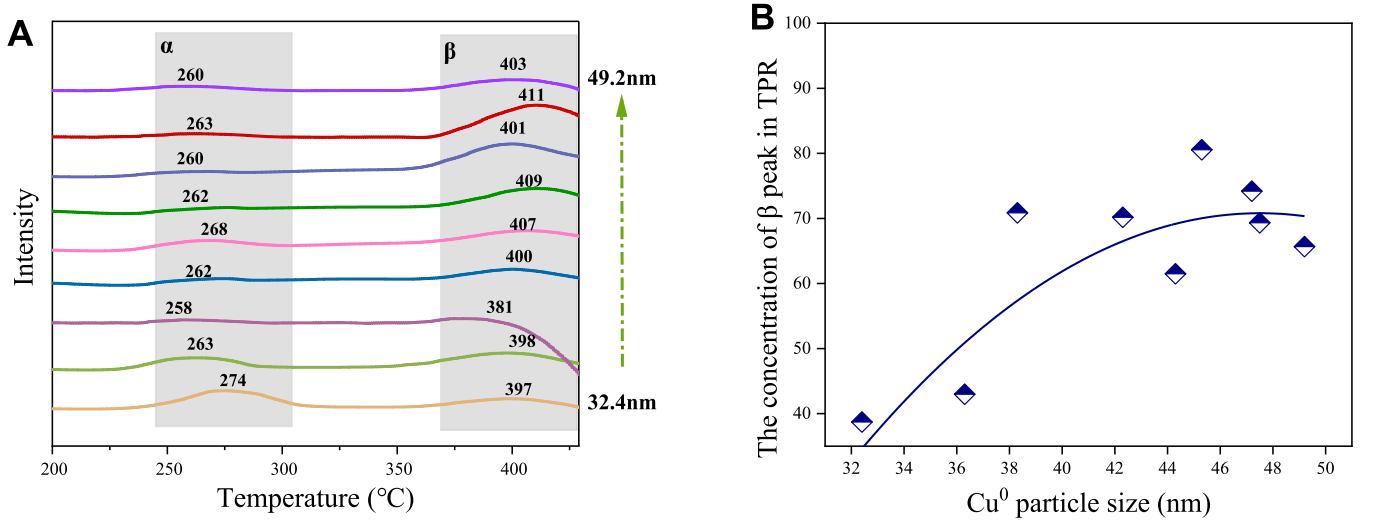

Fig. 5. H_2-TPR profiles of fresh catalyst (A) and H_2 consumption of peak β/α + β calculated by TPR experiments as a function of Cu^0 particle size (B).

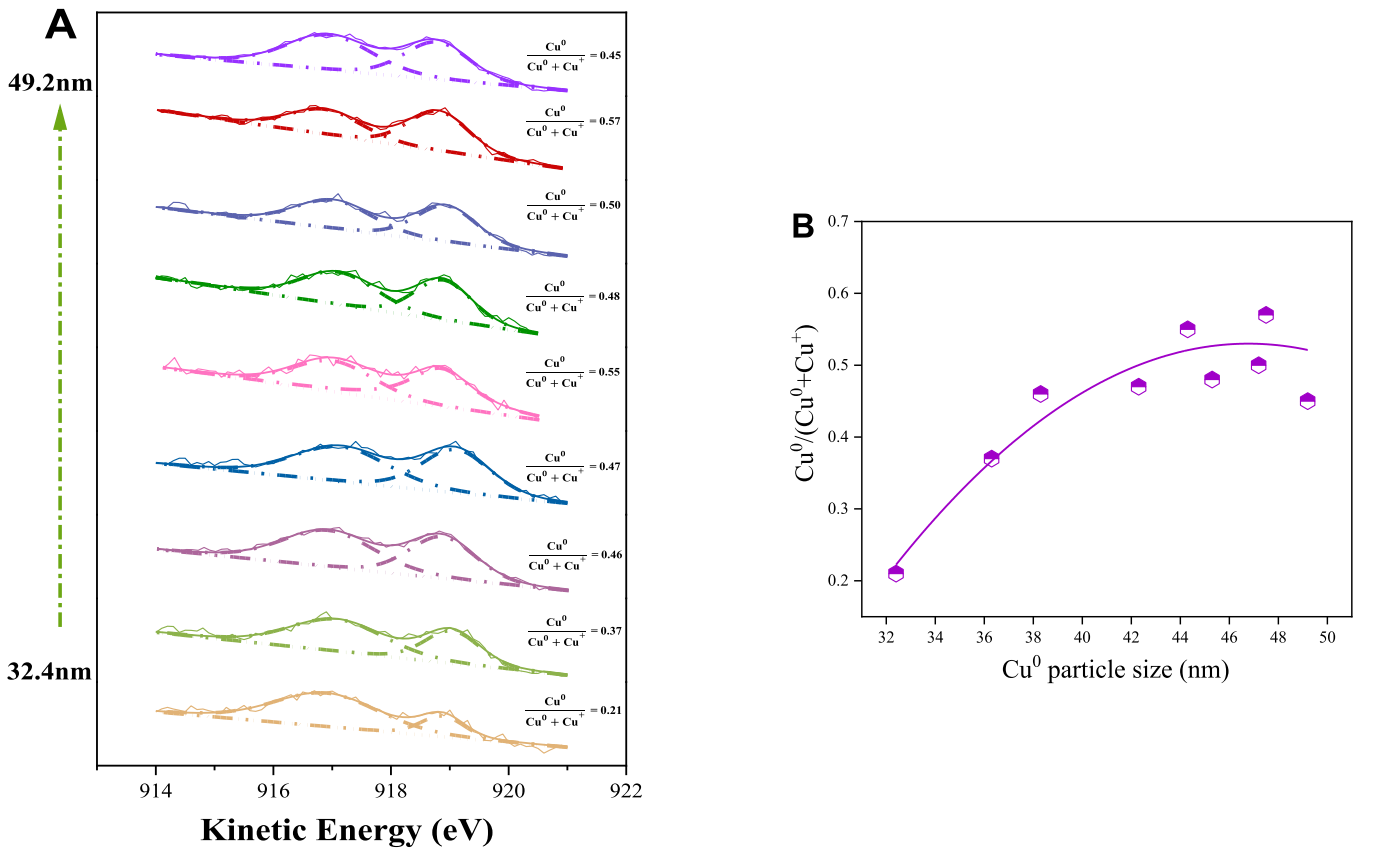

Fig. 6. Deconvolution of Cu LMM X-ray excited auger spectroscopy of fresh catalysts and the ratios of $Cu^0/(Cu^0+Cu^+)$ as a function of Cu^0 particle size.

et al. [54] who believed that CO mainly existed in the bridge-adsorbed site on larger Rh particles. Thus, it was easy to understand that the $C_{2+}OH$ could be formed from CO hydrogenation at larger Cu particle size and the reaction was highly size-dependent.

The surface intermediates and possible reaction pathway evolved in the reaction were elucidated to understand the mechanism by *in-situ* DRIFTS of $CO+H_2$ experiment on the CuZnAl catalysts with different Cu particle size at 250 and 280 ℃, 0.1 MPa and $H_2/CO= 2$. As shown in Fig. 8A and Fig. S11, several intermediates such as CH_x* , CHO* / CH_3O* , CH_3CO* /CH_3CHO* /CH_3CH_2O* , CH_3COO* /HCOO* and gaseous CH_4 were detected. The peaks located at 3030–3034 cm^{-1} and 1574 cm^{-1} were attributed to the C-H and C-O bond of CHO* from initial CO hydrogenation [55,56]. The bands situated at 3012 cm^{-1} and 2920 cm^{-1} were attributed to saturated C-H bond in CH_4 and unsaturated C-H bond in CH_x* (e.g. CH_2 *), respectively [56,57]. The formation of CH_x* and CH_4 confirmed the dissociation of C-O bond on the catalyst surface, and the former was regarded to be the key intermediates deriving from the adsorbed bri-CO in ethanol synthesis process. In addition, the precursors of ethanol including aldehyde species (CH_3CHO*, 2850, 1440 cm^{-1}) and ethoxy species (CH_3CH_2O*, 2952, 2874 cm^{-1}) and ketene species (CH_2CO*, 1650, 1253 cm^{-1}) were detected [57–59], confirming the C-C coupling occurred via CO* /CHO* insertion mechanism, which was consistent with previous DFT calculations on Cu-based catalyst and Cu modified F-T catalyst [19, 60]. Interestingly, several new bands of formate species (HCOO*, 2860, 1360 cm^{-1}) and acetate species (CH_3COO*, 1760, 1560, 1470 cm^{-1}) were also emerged [55,58]. The HCOO* might be due to the hydrogenation of gaseous CO_2 which was originated from water-gas shift reaction (WGS: $CO+H_2O \rightarrow CO_2 + H_2$), while the CH_3COO* should be from the coupling of CH_x* and CO_2 * (CH_x*+CO_2 *→CH_xCOO*+ *) [57,58]. This new reaction pathways by coupling of CH_x* and CO_2 * and followed by hydrogenation to form ethanol were also discovered by Ding's group in CO_2 hydrogenation reaction [61]. The above work indicated that there were three possible pathways for ethanol synthesis on CuZnAl catalyst: (a) the non-dissociative adsorbed CO was firstly hydrogenated to form CHO* species which coupled with CH_x* to form CH_3CH_xO* and then further hydrogenated to produce ethanol; (b): the adsorbed CO* species was directly inserted into the CH_x* species to form CH_2CO* intermediates which further hydrogenated to complete the ethanol synthesis. (c): the CO_2 was firstly produced from the WGS reaction on Cu sites, followed by coupling of CH_x* and CO_2 * to form CH_xCOO* which could be hydrogenated to yield ethanol with CH_xCHO* species as the intermediate (CH_xCOO* + 2 H* → CH_xCHO* + OH*).

Additionally, it could be seen from Fig. 8B that the characteristic peaks intensity of CH_x* at 2920 cm^{-1} significantly enhanced with the increase of Cu particle size, indicating that increasing Cu particle size could significantly prevented the hydrogenation of CH_x* to CH_4, thus increasing the coverage of CH_x* intermediates and extending its retention time. Meanwhile, we could also found that the peak intensity of CHO* at 3034 cm^{-1} to the band of CH_3O*at 1418 cm^{-1} increased with increasing Cu particle size, indicating that the CHO* species was not conducive to directly hydrogenated to form CH_3O* and further hydrogenation to yield CH_3OH, but it was more likely to coupled with CH_x*to form CH_3CHO* intermediates at larger Cu particle size. This phenomenon was consistent with the relative higher coverage of CH_3CHO* at 2850 cm^{-1} in CuZnAl catalyst with Cu particle size of 47.5 nm. The increased coverage of C_{2+} precursors and the CH_x*intermediates as well as the decreased CH_3O* concentration in catalyst with larger Cu particle size could simultaneously result in the higher fraction of $C_{2+}OH/ROH$, which was also account for the enhanced chain growth ability when increasing Cu particle size. Furthermore, one could also see that the temperature seemed to have a greater effect on surface intermediates when decreasing Cu particle size because from 250 ℃ to 280 ℃, the

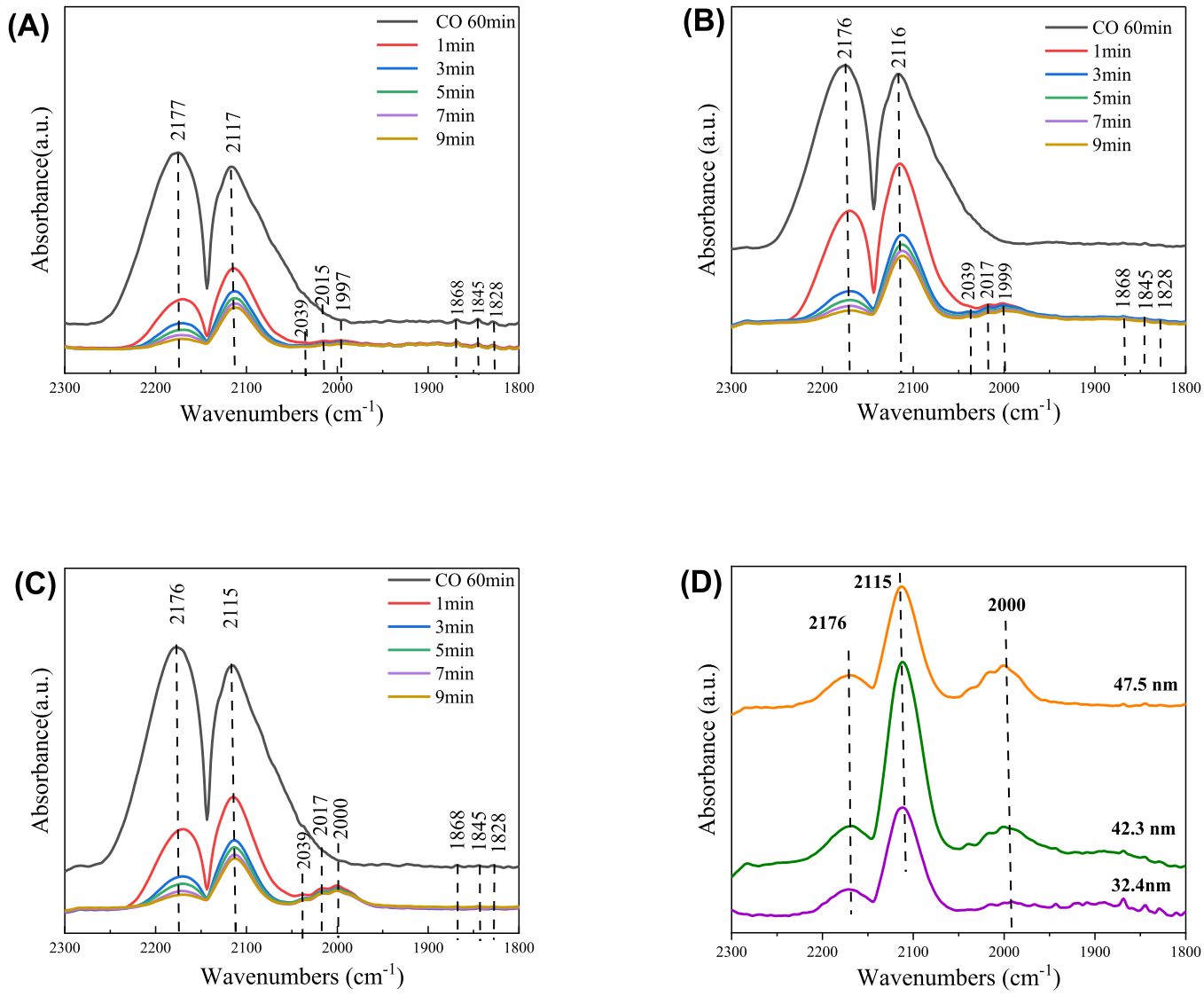

Fig. 7. *In-situ* DRIFTS spectra of CO adsorption at 523 K and then in Ar for 1 min, 3 min, 5 min, 7 min and 9 min over catalyst with Cu particle size of 32.4 nm (a); 42.3 nm (b); 47.5 nm (c). The IR signal of various catalysts after 9 min Ar flushing (d).

surface intermediates varied more obviously at smaller Cu particle size.

3.4. Discussion

The catalytic conversion of CO_x ($x = 1, 2$) hydrogenation to alcohols was a complex and structure-sensitive process. The dependence of the catalytic activity and selectivity on the active phase and particle size was an idiosyncrasy of the reactions. For the Cu-based methanol synthesis reaction, several articles found a linear correlation between the activity and the exposed Cu^0 surface area determined by N_2O adsorption [47,62]. In addition, it was reported that the surface-specific activity significantly decreased when copper particles was smaller than 8 nm since the fraction of atoms with lower coordination numbers increasing [63]. DFT calculation suggested that the lower total energy barrier dominated due to the increase of more unsaturated surface sites, which changed the percentage of specific step sites, thus leading to particle size effect [64]. Moreover, some studies showed that the formation rate of methanol was sensitive to Cu (100), Cu (110) and Cu (111) single crystals [65,66], and the $Cu_{Cu(611)}Zn$ alloy was identified the active sites of Cu-ZnO catalysts for CO hydrogenation reactions [20].

However, our previous studies demonstrated that CuZnAl catalyst prepared by CLP technology exhibited high selectivity to ethanol [13]. The ratio of $Cu^0/(Cu^0+Cu^+)$, AlOOH, and the oxygen vacancies of ZnO_x, as well as the structural differentiation between the CuZnAl catalyst prepared by the CLP technology and the industrial methanol synthesis catalyst therefore have been studied in detail [14,21,67–69]. All these studies suggested the relatively larger Cu particle size of catalyst prepared by the CLP technology was the most significant feature compared with other Cu-based methanol synthesis catalyst, and did not denied the effect of Cu particle size. To further investigate the effect of Cu particle size on the syngas to ethanol reaction, it was necessary to controllably synthesize Cu nanostructures with different sizes. However, due to the original innovation of the CLP technology and the limited methods available for reference, it was quite challenging to synthesize catalysts with different Cu particle sizes in a liquid paraffin environment and these obtained Cu particles tend to become smaller when it was placed in the slurry bed reactor with continuous stirred. Thus, we tried to adjust the loading of Cu and Zn, and successfully synthesized the narrow distribution Cu particle with size of 32.4–49.2 nm.

It was very interesting to find that relative larger Cu particle size exhibited similar function of F-T element (e.g. Fe, Co) on ethanol formation, while smaller Cu particle size favored to methanol formation from CO hydrogenation. In this study, the selectivity of ethanol and $C_{2+}OH$ increased dramatically above a certain critical particle size

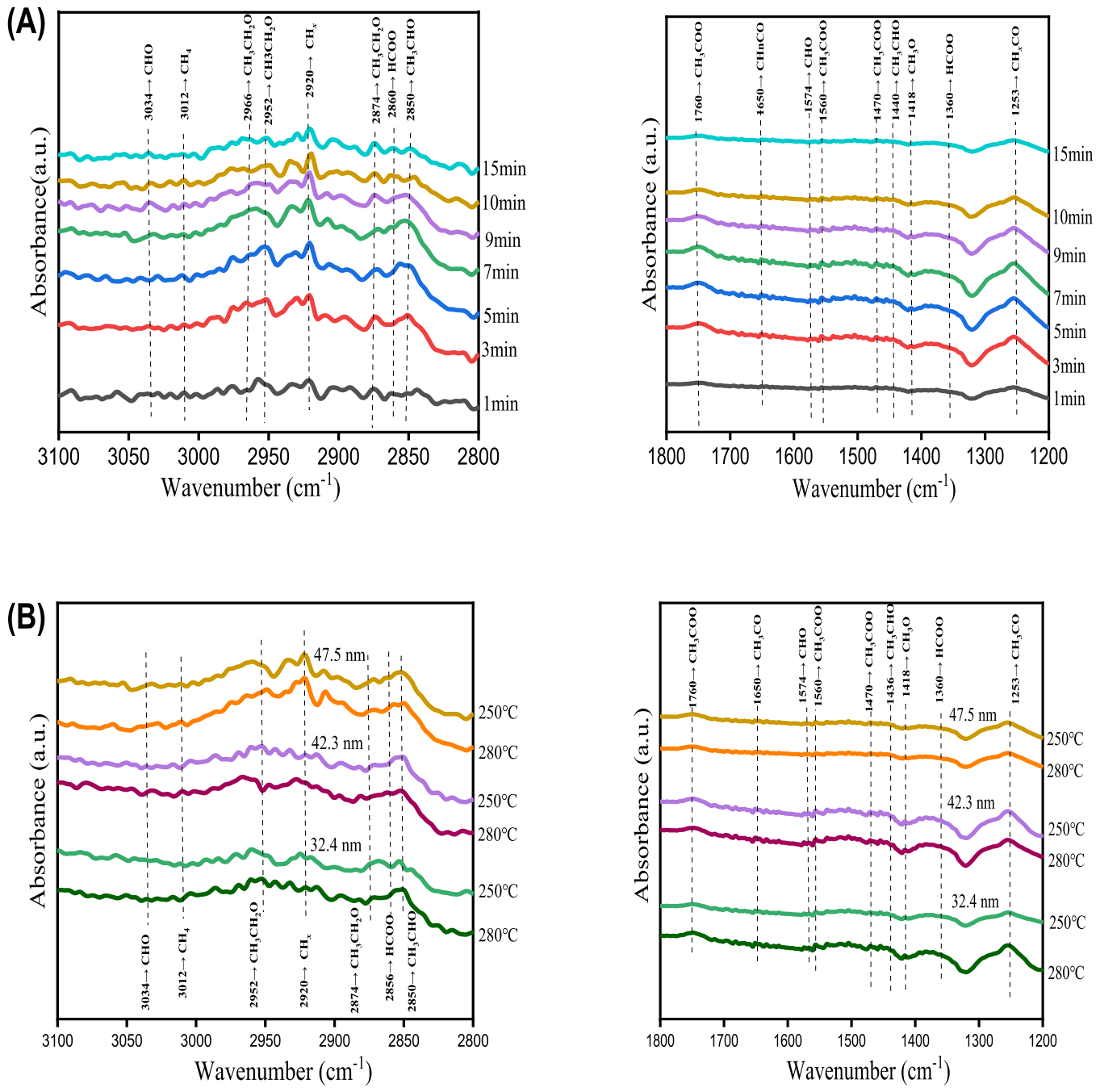

Fig. 8. *In-situ* DRIFTS spectra of CO+H_2 reaction over catalyst with Cu particle size of 47.5 nm (A) and the comparison of IR signal on catalysts with different Cu particle size (B).

(~38.3 nm) for CuZnAl catalyst, which ensured the C_{2+}OH selectivity was more than 50%, while the methanol and DME selectivity showed the opposite trend. The relationship between the particle size of Cu and CH_x selectivity, which represented the CO dissociation ability of the catalyst, also suggested that there was a certain critical particle size of Cu at about 38.3 nm. These results indicated that the structure of Cu in larger particles had changed significantly, and new active sites might have been created. In addition, the apparent activation energy (E_a) increased sharply when the size increased to 38.3 nm, which further indicated the effect of Cu particle size on kinetics of syngas to ethanol and higher alcohols. It was speculated that the higher E_a for Cu particle with larger size leads to the weaker activity of hydrogenation because the hydrogenation process of CH_xO* was observed to be blocked according to our previous study [21]. As a result, C-C coupling was enhanced, leading to a raise of selectivity to C_{2+}OH. Unfortunately, it was impossible for us to carry out relevant density functional theory (DFT) research on such large Cu particle sizes. Nonetheless, DFT calculation conducted by Wang's group suggested that the formations of CH_x ($x = 1$–3) was favored on Cu (111) surface, while CH_3OH was more easily formed than CH_3 on Cu (100) for CO hydrogenation to ethanol [17,70]. The above TEM characterization demonstrated that Cu (111) facet dominated the surface at larger Cu particle size and was accompanied by the formation of $Cu_{(111)}$-ZnO interface, which would be conducive to CH_x formation, and the results also had been confirmed by *in-situ* CO-DRIFTS experiments. Wang's group also reported that among all elementary reactions related to CH_3 on Cu surface, inserting CHO into CH_3 to form CH_3CHO was the most favorable pathway, followed by the formation of CH_3CO, while CH_2, CH_4 and C_2H_6 were hard to generate due to the high

activation barrier [71]. Based on the results of *in-situ* DRIFTS results, a plausible mechanism for ethanol and $C_{2+}OH$ synthesis over CuZnAl catalyst was summarized in Scheme 1. The non-dissociative CO was firstly hydrogenated to form CHO* species which was further hydrogenated to yield CH_3OH via CH_3O* intermediate on relative smaller Cu particle size (e.g. 11.8 nm). The C-O bond of bri-CO could be split on $Cu_{(111)}$-ZnO interface at larger Cu sizes (e.g. 47.5 nm) and thus resulted in the formation of CH_x* intermediates. These CH_x* could couple with each other and further hydrogenated to form a long-chain hydrocarbon, or by the insertion of CHO* /CO* to form CH_3CHO* /CH_2CO* which further hydrogenated to obtain the ethanol/$C_{2+}OH$ on Cu sites. Apart from the insertion mechanism, we also proposed the possibility of ethanol synthesis via CH_3COO* intermediate which was derived from the coupling of CH_x* and CO_2 * (CH_x*+CO_2 *→CH_xCOO* + *), and it would further hydrogenated to yield ethanol with aldehyde (e.g. CH_3CHO*) as intermediate (2 H*+CH_3COO*→CH_3CHO* + OH*).

Finally, to achieve high selectivity and yield of ethanol from syngas on Cu-based catalyst, it was necessary to selectively modify Cu catalyst to depress the negative influence of other active sites by using the promoters (e.g. K, Mn, In), thereby boost CH_3 formation and/or suppress CH_3OH and hydrocarbon formation. Besides, considering that the formation of ethanol and $C_{2+}OH$ was always accompanied by the formation of water, the presence of water then would change the size of Cu particle, thereby affecting the catalyst stability. As depicted in Fig. 3D, the selectivity of CO_2 increased obviously after 370 h. Therefore, further design carbon-encapsulated hydrophobic Cu-based catalyst might be necessary. The encapsulated hydrophobic structure not only protected Cu from the influence of water, thereby stabilizing Cu particles, and was even expected to solve the high selectivity of CO_2. It also favored to enhance the strong electronic interaction between the metallic Cu and the carbon layer, thereby promoting the improvement of activity. However, this would rely on available synthesis technologies for the synthesis of size-controlled Cu particle.

4. Conclusions

In conclusion, we have successfully fabricated a series of CuZnAl catalysts with narrow distribution Cu particle sizes of 32.4–49.2 nm by CLP technology to investigate the size-dependent of Cu particle in syngas to ethanol and higher alcohols synthesis. The selectivity towards to higher alcohols sharply increased from 8.9% to 60.5% with the increase of Cu particle size from 11.8 to 38.3 nm, then it slightly increased to the value of about 68.6% when further increasing the Cu particle size to 49.2 nm, while the CO conversion slightly decreased with the increase of Cu particle size overall. Smaller Cu particle size possessed relative larger exposed copper surface area (S_{Cu}) for hydrogenation, while Cu (111) facet dominated the surface of larger Cu particle size and was accompanied by the formation of $Cu_{(111)}$-ZnO interface, thus was conducive to the C-O bond dissociation for CH_x formation. *In-situ* DRIFTS experiment confirmed, apart from the insertion of CO* /CHO* into the CH_x* intermediate for carbon chain growth, the possibility of ethanol synthesis over Cu-based catalyst also could be derived from the coupling of CH_x* and CO_2 * to form CH_xCOO* which was further hydrogenated to yield ethanol with aldehyde as intermediate. Our findings substantially broaden the understanding the size effect of Cu on syngas conversion as well as carbon chain growth mechanism, and provided significant guidance for design of more active copper-based catalyst for ethanol synthesis.

CRediT authorship contribution statement

Wei Huang designed this work and Yongjun Liu prepared the catalysts, wrote the paper and analyzed the data. The catalyst characterizations were conducted by Zhiwen Li, while the in-situ DRIFTS measurement was conducted by Peng Luo. Catalytic activity measurement was carried out by Nan Cui, and Kejing Wang provided some valuable discussions.

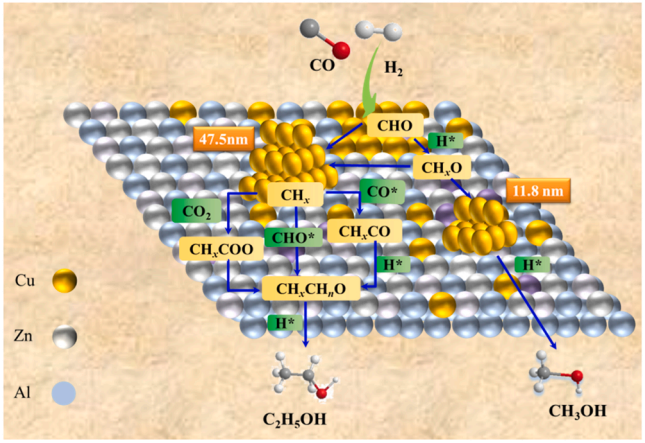

Scheme 1. Proposed reaction mechanism of ethanol synthesis from syngas over CuZnAl catalyst.

Declaration of Competing Interest

The authors declare that they have no known competing financial interests or personal relationships that could have appeared to influence the work reported in this paper.

Data Availability

Data will be made available on request.

Acknowledgements

The authors gratefully acknowledge the National Natural Science Foundation of China (21908157), Natural Science Younger Foundation of Shanxi Province (201801D221076), Shanxi Provincial Key Research and Development Project (201803D121043), and Shanxi-Zheda Institute of Advanced Materials and Chemical Engineering (2021SX-FR009).

Appendix A. Supporting information

Supplementary data associated with this article can be found in the online version at doi:10.1016/j.apcatb.2023.122949.

References

[1] W. Zhou, K. Cheng, J. Kang, C. Zhou, V. Subramanian, Q. Zhang, Y. Wang, New horizon in C1 chemistry: breaking the selectivity limitation in transformation of syngas and hydrogenation of CO_2 into hydrocarbon chemicals and fuels, Chem. Soc. Rev. 48 (2019) 3193–3228.
[2] N. Li, F. Jiao, X.L. Pan, Y.X. Chen, J.Y. Feng, G. Li, X.H. Bao, High-quality gasoline directly from syngas by dual metal oxide-zeolite (OX-ZEO) catalysis, Angew. Chem. Int. Ed. 58 (2019) 7400–7404.
[3] H.M.T. Galvis, K.P. de Jong, Catalysts for production of lower olefins from synthesis gas: a review, ACS Catal. 3 (2013) 2130–2149.
[4] F. Jiao, J.J. Li, X.L. Pan, J.P. Xiao, H.B. Li, H. Ma, M.M. Wei, Y. Pan, Z.Y. Zhou, M. R. Li, S. Miao, J. Li, Y.F. Zhu, D. Xiao, T. He, J.H. Yang, F. Qi, Q. Fu, X.H. Bao, Selective conversion of syngas to light olefins, Science 351 (2016) 1065–1068.
[5] S. Kasipandi, J.W. Bae, Recent advances in direct synthesis of value-added aromatic chemicals from syngas by cascade reactions over bifunctional catalysts, Adv. Mater. 31 (2019) 1803390.
[6] Y.P. Chen, J.T. Wei, M.S. Duyar, V.V. Ordomsky, A.Y. Khodakov, J. Liu, Carbon-based catalysts for Fischer-Tropsch synthesis, Chem. Soc. Rev. 50 (2021) 2337–2366.
[7] C. Huang, C. Zhu, M.W. Zhang, J.G. Chen, K.G. Fang, Design of efficient ZnO/ZrO_2 modified CuCoAl catalysts for boosting higher alcohol synthesis in syngas conversion, Appl. Catal. B: Environ. 300 (2022), 120739.
[8] Y.W. Li, W. Gao, M. Peng, J.B. Zhang, J. Sun, Y. Xu, S. Hong, X. Liu, X.W. Liu, M. Wei, B.S. Zhang, D. Ma, Interfacial Fe_5C_2-Cu catalysts toward low-pressure syngas conversion to long-chain alcohols, Nat. Commun. 11 (2020) 61.

[9] M. Gupta, M.L. Smith, J.J. Spivey, Heterogeneous catalytic conversion of dry syngas to ethanol and higher alcohols on Cu-based catalysts, ACS Catal. 1 (2011) 641–656.

[10] G. Prieto, S. Beijer, M.L. Smith, M. He, Y. Au, Z. Wang, D.A. Bruce, K.P. de Jong, J. J. Spivey, P.E. de Jongh, Design and synthesis of copper-cobalt catalysts for the selective conversion of synthesis gas to ethanol and higher alcohols, Angew. Chem. Int. Ed. 53 (2014) 6397–6401.

[11] T.J. Lin, X.Z. Qi, X.X. Wang, L. Xia, C.Q. Wang, F. Yu, H. Wang, S.G. Li, L.S. Zhong, Y.H. Sun, Direct production of higher oxygenates by syngas conversion over a multifunctional catalyst, Angew. Chem. Int. Ed. 58 (2019) 4627–4631.

[12] G.B. Liu, G.H. Yang, X.B. Peng, J.H. Wu, N. Tsubaki, Recent advances in the routes and catalysts for ethanol synthesis from syngas, Chem. Soc. Rev. 51 (2022) 5606–5659.

[13] W. Huang, L. Yu, W. Li, Z. Ma, Synthesis of methanol and ethanol over CuZnAl slurry catalyst prepared by complete liquid-phase technology, Front. Chem. Eng. China 4 (2010) 472–475.

[14] Y.T. Gu, C. Han, J.H. Huang, V.A. Vinokurov, W. Huang, CuZnAlOOH catalysts with Cu^0/Cu^+ constructed by two-step hydrolysis for ethanol production from syngas, Fuel 322 (2022), 124111.

[15] B. Bai, H. Bai, L. Zhang, W. Huang, Catalytic activity of γ-AlOOH (001) surface in syngas conversion: probing into the mechanism of carbon chain growth, Appl. Surf. Sci. 455 (2018) 123–131.

[16] Y.J. Liu, X. Deng, P.D. Han, W. Huang, CO hydrogenation to higher alcohols over CuZnAl catalysts without promoters: effect of pH value in catalyst preparation, Fuel Process. Technol. 167 (2017) 575–581.

[17] H.Y. Zheng, R.G. Zhang, Z. Li, B.J. Wang, Insight into the mechanism and possibility of ethanol formation from syngas on Cu(100) surface, J. Mol. Catal. A: Chem. 404 (2015) 115–130.

[18] R.G. Zhang, G.R. Wang, B.J. Wang, Lixia Ling, Insight into the effect of promoter Mn on ethanol formation from syngas on a Mn-promoted MnCu(211) surface: A comparison with a Cu(211) surface, J. Phys. Chem. C. 118 (2014) 5243–5254.

[19] R.G. Zhang, X.C. Sun, Baojun Wang, Insight into the preference mechanism of CH*x* (x=1-3) and C-C chain formation involved in C2 oxygenate formation from syngas on the Cu(110) surface, J. Phys. Chem. C. 117 (2013) 6594–6606.

[20] Z.H. Zhang, X.Y. Chen, J.C. Kang, Z.Y. Yu, J. Tian, Z.M. Gong, A.P. Jia, R. You, K. Qian, S. He, B.T. Teng, Y. Cui, Y. Wang, W.H. Zhang, W.X. Huang, The active sites of Cu-ZnO catalysts for water gas shift and CO hydrogenation reactions, Nat. Commun. 12 (2021) 4331.

[21] P.L. Jia, Y.J. Liu, R. Yang, P. Luo, W. Huang, Insight into the structural sensitivity of CuZnAl catalysts for CO hydrogenation to alcohols, Fuel 323 (2022), 124265.

[22] S. Natesakhawat, J.W. Lekse, J.P. Baltrus, P.R. Ohodnicki, B.H. Howard, X.Y. Deng, C. Matranga, Active sites and structure-activity relationships of copper-based catalysts for carbon dioxide hydrogenation to methanol, ACS Catal. 2 (2012) 1667–1676.

[23] A. Karelovic, P. Ruiz, The role of copper particle size in low pressure methanol synthesis via CO_2 hydrogenation over Cu/ZnO catalysts, Catal. Sci. Technol. 5 (2015) 869–881.

[24] N. Li, F. Jiao, X.L. Pan, Y. Ding, J.Y. Feng, X.H. Bao, Size effects of ZnO nanoparticles in bifunctional catalysts for selective syngas sonversion, ACS Catal. 9 (2019) 960–966.

[25] Y.Y. Dai, Y.H. Zhao, T.J. Lin, S.G. Li, F. Yu, Y.L. An, X.X. Wang, K. Xiao, F.F. Sun, Z. Jiang, Y.W. Lu, H. Wang, L.S. Zhong, Y.H. Sun, Particle size effects of cobalt carbide for Fischer-Tropsch to olefins, ACS Catal. 9 (2019) 798–809.

[26] J.L. Gong, H.R. Yue, Y.J. Zhao, S. Zhao, L. Zhao, J. Lv, S.P. Wang, X.B. Ma, Synthesis of ethanol via syngas on Cu/SiO_2 catalysts with balanced Cu^0-Cu^+ sites, J. Am. Chem. Soc. 134 (2012) 13922–13925.

[27] Y.J. Liu, X. Deng, L. Jia, W. Huang, Investigation of copper precursors in the synthesis of higher alcohols from syngas over CuZnAl catalysts without promoters, Phys. Chem. Chem. Phys. 20 (2018) 18790–18799.

[28] P. Luo, Y.J. Liu, K.J. Wang, Z.W. Li, C.Y. Zhang, Y.X. Wu, X.Y. Zan, W. Huang, Investigation of Al precursor for ethanol synthesis from syngas on Cu-based multifunctional catalyst, Fuel Process. Technol. 245 (2023), 107728.

[29] J. Sun, J.F. Yu, Q.X. Ma, F.Q. Meng, X.X. Wei, Y.N. Sun, N. Tsubaki, Freezing copper as a noble metal-like catalyst for preliminary hydrogenation, Sci. Adv. 4 (2018) eaau3275.

[30] Y.J. Liu, N. Cui, P.L. Jia, X. Wang, W. Huang, Synergy between active sites of ternary CuZnAlOOH catalysts in CO hydrogenation to ethanol and higher Alcohols, ACS Sustain, Chem. Eng. 8 (2020) 6634–6646.

[31] M. Behrens, F. Studt, I. Kasatkin, S. Kuhl, M. Havecker, F. Abild-Pedersen, S. Zander, F. Girgsdies, P. Kurr, B.L. Kniep, M. Tovar, R.W. Fischer, J.K. Norskov, R. Schlogl, The active site of methanol synthesis over $Cu/ZnO/Al_2O_3$ industrial catalysts, Science 336 (2012) 893–897.

[32] J.F. Xu, W. Ji, Z.X. Shen, W.S. Li, S.H. Tang, X.R. Ye, D.Z. Jia, X.Q. Xin, Raman spectra of CuO nanocrystals, J. Raman Spectrosc. 30 (1999) 413–415.

[33] V. Russo, M. Ghidelli, P. Gondoni, C.S. Casari, A.L. Bassi, Multi-wavelength Raman scattering of nanostructured Al-doped zinc oxide, J. Appl. Phys. 115 (2014), 073058.

[34] A.G. Milekhin, N.A. Yeryukov, L.L. Sveshnikova, T.A. Duda, C. Himcinschi, E. I. Zenkevich, D.R.T. Zahn, Resonant Raman scattering of ZnS, ZnO, and ZnS/ZnO core/shell quantum dots, Appl. Phys. A-Mater. Sci. Process 107 (2012) 275–278.

[35] D.S. Zhang, C. Zhang, J. Liu, Q. Chen, X.G. Zhu, C.H. Liang, Carbon-encapsulated metal/metal carbide/metal oxide core-shell nanostructures generated by laser ablation of metals in organic solvents, ACS Appl. Nano Mater. 2 (2019) 28–39.

[36] D. Uzio, G. Berhault, Factors governing the catalytic reactivity of metallic nanoparticles, Catal. Rev. Sci. Eng. 52 (2010) 106–131.

[37] S. Kuld, M. Thorhauge, H. Falsig, C.F. Elkjaer, S. Helveg, I. Chorkendorff, J. Sehested, Quantifying the promotion of Cu catalysts by ZnO for methanol synthesis, Science 352 (2016) 969–974.

[38] J. Yoshihara, C.T. Campbell, Methanol synthesis and reverse water-gas shift kinetics over Cu(110) model catalysts: structural sensitivity, J. Catal. 161 (1996) 776–782.

[39] L.C. Grabow, M. Mavrikakis, Mechanism of methanol synthesis on Cu through CO_2 and CO hydrogenation, ACS Catal. 1 (2011) 365–384.

[40] C. Price, L. Pastor-Perez, E. le Sache, A. Sepulveda-Escribano, T.R. Reina, Highly active Cu-ZnO catalysts for the WGS reaction at mediumehigh space velocities: effect of the support composition, Int. J. Hydrog. Energ. 42 (2017) 10747–10751.

[41] N. Liu, M. Xu, Y.S. Yang, S.M. Zhang, J. Zhang, W.L. Wang, L.R. Zheng, Song Hong, Min Wei, Au^{δ}-O_v-Ti^{3+} interfacial site: catalytic active center toward low-temperature water gas shift reaction, ACS Catal. 9 (2019) 2707–2717.

[42] L.D. Gao, Y. Tang, Q.S. Xue, Y. Liu, Y. Lu, Hydrotalcite-like compounds derived CuZnAl oxide catalysts for aerobic oxidative removal of gasoline-range organosulfur compounds, Energy Fuels 23 (2009) 624–630.

[43] B.V. Farahani, F.H. Rajabi, M. Bahmani, M. Ghelichkhani, S. Sahebdelfar, Influence of precipitation conditions on precursor particle size distribution and activity of Cu/ZnO methanol synthesis catalyst, Appl. Catal. A: Gen. 482 (2014) 237–244.

[44] C. Baltes, S. Vukojevic, F. Schuth, Correlations between synthesis, precursor, and catalyst structure and activity of a large set of $CuO/ZnO/Al_2O_3$ catalysts for methanol synthesis, J. Catal. 258 (2008) 334–344.

[45] P. Gao, F. Li, H.J. Zhan, N. Zhao, F.K. Xiao, W. Wei, L.S. Zhong, H. Wang, Y.H. Sun, Influence of Zr on the performance of Cu/Zn/Al/Zr catalysts via hydrotalcite-like precursors for CO_2 hydrogenation to methanol, J. Catal. 298 (2013) 51–60.

[46] T. Herranz, X.Y. Deng, A. Cabot, J.G. Guo, M. Salmeron, Influence of the cobalt particle size in the CO hydrogenation reaction studied by in situ X-ray absorption spectroscopy, J. Phys. Chem. B. 113 (2009) 10721–10727.

[47] M.L. Smith, N. Kumar, J.J. Spivey, C.O. Adsorption, Behavior of Cu/SiO_2, Co/SiO_2, and $CuCo/SiO_2$ catalysts studied by in situ DRIFTS, J. Phys. Chem. C. 116 (2012) 7931–7939.

[48] K.I. Hadjiivanov, G.N. Vayssilov, Characterization of oxide surfaces and zeolites by carbon monoxide as an IR probe molecule, Adv. Catal. 47 (2002) 307–511.

[49] F. Bin, X.L. Wei, B. Li, K.S. Hui, Self-sustained combustion of carbon monoxide promoted by the Cu-Ce/ZSM-5 catalyst in $CO/O_2/N_2$ atmosphere, Appl. Catal. B: Environ. 162 (2015) 282–288.

[50] Y. Wang, Y.L. Shen, Y.J. Zhao, J. Lv, S.P. Wang, X.B. Ma, Insight into the balancing effect of active Cu species for hydrogenation of carbon-oxygen bonds, ACS Catal. 5 (2015) 6200–6208.

[51] J. Schumann, J. Krohnert, E. Frei, R. Schlogl, A. Trunschke, IR-spectroscopic study on the interface of Cu-based methanol synthesis catalysts: evidence for the formation of a ZnO overlayer, Top. Catal. 60 (2017) 1735–1743.

[52] N. Kapur, J. Hyun, B. Shan, J.B. Nicholas, K. Cho, Ab initio study of CO hydrogenation to oxygenates on reduced Rh terraces and stepped surfaces, J. Phys. Chem. C. 114 (2010) 10171–10182.

[53] K. Sun, M.H. Tan, Y.X. Bai, X.F. Gao, P. Wang, N.N. Gong, T. Zhang, G.H. Yang, Y. S. Tan, Design and synthesis of spherical-platelike ternary copper-cobalt-manganese catalysts for direct conversion of syngas to ethanol and higher alcohols, J. Catal. 378 (2019) 1–16.

[54] A. Hironori, F. Takakazu, I. Masaru, T. Kazuhiko, M. Takehiko, S. Yoshihiro, High pressure in-situ FT-IR study of CO hydrogrnation over Rh/SiO_2 catalyst, Chem. Lett. 14 (1985) 23–26.

[55] Z. Zeng, Z.S. Li, T. Guan, S.X. Guo, Z.W. Hu, J.H. Wang, A. Rykov, J. Lv, S. Y. Huang, Y. Wang, X.N. Ma, CoFe alloy carbide catalysts for higher alcohols synthesis from syngas: evolution of active sites and Na promoting effect, J. Catal. 405 (2022) 430–444.

[56] C.T. Wang, J. Zhang, G.Q. Qin, L. Wang, E. Zuidema, Q. Yang, S.S. Dang, C. G. Yang, J.P. Xiao, X.J. Meng, C. Mesters, F.S. Xiao, Direct conversion of syngas to ethanol within zeolite crystals, Chem 6 (2020) 646–657.

[57] W.X. Qian, H. Wang, Y.B. Xu, X.L. Yang, G.W. Zhai, H.T. Zhang, H.F. Ma, Q.W. Sun, W.Y. Ying, In situ DRIFTS study of homologous reaction of methanol and higher alcohols synthesis over Mn promoted Cu-Fe catalysts, Ind. Eng. Chem. Res. 58 (2019) 6288–6297.

[58] Y. Wang, K.Z. Wang, B.Z. Zhang, X.B. Peng, X.H. Gao, G.H. Yang, H. Hu, M.B. Wu, N. Tsubaki, Direct conversion of CO_2 to ethanol boosted by intimacy-sensitive multifunctional catalysts, ACS Catal. 11 (2021) 11742–11753.

[59] Z. Zeng, Z.S. Li, S.X. Guo, J. Lv, S.Y. Huang, Y. Wang, X.B. Ma, Janus Au-$Fe_{2.2}C$ catalyst for direct conversion of syngas to higher alcohols, ACS Sustain, Chem. Eng. 9 (2021) 11258–11268.

[60] Y.W. Lu, R.G. Zhang, B.B. Cao, B.H. Ge, F.F. Tao, J.J. Shan, L. Nguyen, Z.H. Bao, T. P. Wu, J.W. Pote, B.J. Wang, F. Yu, Elucidating the copper-hägg iron carbide synergistic interactions for selective CO hydrogenation to higher alcohols, ACS Catal. 7 (2017) 5500–5512.

[61] L.P. Ding, T.T. Shi, J. Gu, Y. Cui, Z.Y. Zhang, C.J. Yang, T. Chen, M. Lin, P. Wang, N.H. Xue, L.M. Peng, X.F. Guo, Y. Zhu, Z.X. Chen, W.P. Ding, CO_2 hydrogenation to ethanol over Cu@Na-Beta, Chem 6 (2020) 2673–2689.

[62] M. Kurtz, H. Wilmer, T. Genger, O. Hinrichsen, M. Muhler, Deactivation of supported copper catalysts for methanol synthesis, Catal. Lett. 86 (2003) 77–80.

[63] R. van den Berg, G. Prieto, G. Korpershoek, L.I. van der Wal, A.J. van Bunningen, S. Laegsgaard-Jorgensen, P.E. de Jongh, K.P. de Jong, Structure sensitivity of Cu and CuZn catalysts relevant to industrial methanol synthesis, Nat. Commun. 7 (2016) 13057.

[64] W.J. van Rensburg, M.A. Petersen, M.S. Datt, J.A. van den Berg, P. van Helden, On the kinetic interpretation of DFT-derived energy profiles: Cu-catalyzed methanol synthesis, Catal. Lett. 145 (2015) 559–568.

[65] P.B. Rasmussen, P.M. Holmblad, T. Askgaard, C.V. Ovesen, P. Stoltze, J.K. Nrskov, I. Chorkendorff, Methanol synthesis on Cu(100) from a binary gas mixture of CO_2 and H_2, Catal. Lett. 26 (1994) 373–381.
[66] J. Yoshihara, S.C. Parker, A. Schafer, C.T. Campbell, Methanol synthesis and reverse water-gas shift kinetics over clean polycrystalline copper, Catal. Lett. 31 (1995) 313–324.
[67] Z.J. Zuo, L. Wang, L.M. Yu, P.D. Han, W. Huang, Experimental and theoretical studies of ethanol synthesis from syngas over CuZnAl catalysts without other promoters, J. Phys. Chem. C. 118 (2014) 12890–12898.
[68] H. Bai, M.M. Ma, B. Bai, H.J. Cao, L. Zhang, Z.H. Gao, V.A. Vinokurov, W. Huang, Carbon chain growth by formyl coupling over the Cu/gamma-AlOOH(001) surface in syngas conversion, Phys. Chem. Chem. Phys. 21 (2019) 148–159.
[69] J. Gong, J. Liu, D.H. Yang, G.K. Guo, J.C. Fan, W. Huang, Cu-Zn synergy for CO hydrogenation to ethanol and methanol on CuZnO catalysts, Catal. Lett. 152 (2022) 2101–2109.
[70] X.C. Sun, R.G. Zhang, B.J. Wang, Insights into the preference of CH_x(x=1-3) formation from CO hydrogenation on Cu(111) surface, Appl. Surf. Sci. 265 (2013) 720–730.
[71] R.G. Zhang, G.R. Wang, B.J. Wang, Insights into the mechanism of ethanol formation from syngas on Cu and an expanded prediction of improved Cu-based catalyst, J. Catal. 305 (2013) 238–255.